SCIENTIFIC REPORTS

OPEN

Tunable and high-sensitivity sensing based on Fano resonance with coupled plasmonic cavities

Yan Deng[1], Guangtao Cao[1,2], Hui Yang[2,3], Guanhai Li[2,3], Xiaoshuang Chen[2,3] & Wei Lu[2,3]

Tunable and high-sensitivity sensing based on Fano resonance is analytically and numerically investigated in coupled plasmonic cavities structure. To analyze and manipulate the Fano line shape, the coupled cavities are taken as a composite cavity that supports at least two resonance modes. A theoretical model is newly-established, and its results agree well with the finite difference time domain (FDTD) simulations for the plasmonic stub-pair structure. The detection sensitivity factor in coupled cavities approaches $6.541 \times 10^7 \, m^{-1}$, which is an order of magnitude larger than single stub case. In addition, the wavelengths of resonant modes in the plasmonic stub-pair structure can be adjusted independently, which paves a new way for improving detection sensitivity. These discoveries hold potential applications for realizing tunable and highly integrated photonic devices.

Fano resonance, originating from destructive interference between narrow discrete state and broad continuum state, exhibits sharp asymmetric profiles and strong field enhancement[1–3], which may benefit enhanced spectroscopy[4], optical switches[5], chemical or biological sensing[6, 7], low-loss waveguiding, and nonlinear optical effects. Surface plasmon polaritons (SPPs) can break the classical diffraction limit and enable manipulating light in sub-wavelength structures, so diverse plasmonic nanostructures such as core-shell nanoparticles[8], ring-disk cavities[9], nano-slits[10, 11] and nanowire lattices[12] have been proposed theoretically and experimentally to achieve Fano resonance. However, the arrayed structures are typically bulky for highly integrated optical circuits, which motivates an ongoing search for ultra-compact plasmonic structure realizing Fano resonance.

Among various plasmonic structures, metal-dielectric-metal (MDM) waveguide, supporting modes with deep subwavelength scale, ease of fabrication, and zero bend losses[13–16], promises the miniaturization of optical devices and has attracted much attention. Recently, the optical properties of MDM waveguide-cavity systems exhibit symmetrical or asymmetrical line shapes, and have been studied by the scattering matrix method[17], transmission line theory[18], quantum-optics approach[19, 20], and temporal coupled-mode theory (CMT)[17, 21], which are considered as a crucial step for development of integrated photonic circuits[22–26]. It is well known that, with variation of nearby or surrounding medium, the transmission and reflection change at fixed wavelength or mode shift can be utilized as sensing signals. In particular, the sharp asymmetrical Fano resonance supported by coupled cavities enables high detection sensitivity in information processing[6, 7, 27–29]. Lu *et al.* demonstrated a nanosensor in MDM waveguide-cavity system[30] and yielded a figure of merit (FOM) of ~500. Chen *et al.* proposed a near-infrared plasmonic refractive index sensor which consists of a fillet cavity coupled with two MDM waveguides[31]. In addition, Huang and co-workers introduced slow-light enhanced refractive index sensor composed of plasmonic MDM waveguide[32]. However, more feasible theoretical model and straightforward approach are desirable to control and tune the spectral response.

In this paper, we numerically and analytically demonstrate tunable and high-sensitivity sensing performances based on Fano resonance in plasmonic coupled cavities system. The coupled cavities are interpreted as a composite cavity, in which the interference between coexisting modes contributes to Fano line shape[20, 33]. A newly-established theoretical model is in good agreement with the FDTD simulations for the plasmonic stub-pair structure. Compared with single cavity case, the coupled plasmonic cavities structure exhibits much sharper asymmetric Fano line shape, and produces an order of magnitude enhancement in detection sensitivity.

[1]College of Physics, Mechanical and Electrical Engineering, Jishou University, Jishou, 416000, China. [2]National Laboratory for Infrared Physics, Shanghai Institute of Technical Physics, Chinese Academy of Sciences, 500 Yu Tian Road, Shanghai, 200083, China. [3]University of Chinese Academy of Science, No. 19A Yuquan Road, Beijing, 100049, China. Correspondence and requests for materials should be addressed to Y.D. (email: yanzi1232@126.com) or G.L. (email: ghli0120@mail.sitp.ac.cn).
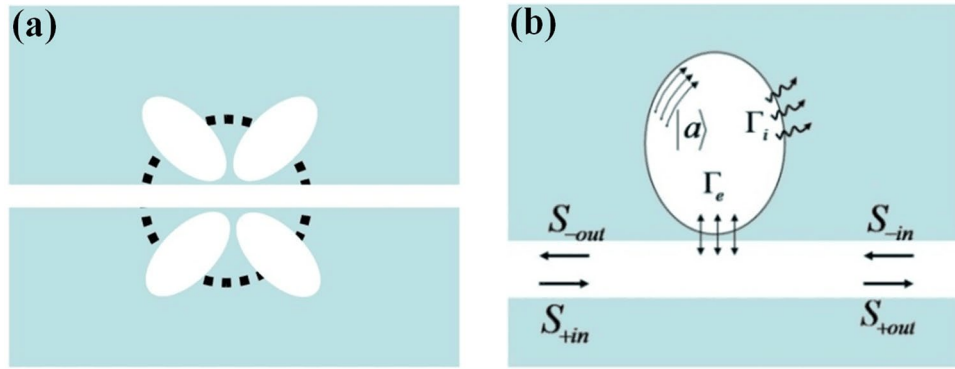
1

Figure 1. (**a**) Schematic of waveguide coupled to multiple cavities. (**b**) Schematic of theoretical model.

Moreover, the resonant positions of bright mode and dark mode in the stub-pair structure can be adjusted independently, which promises solutions for realizing and tuning the high detection sensitivity.

Theoretical model

Figure 1(a) shows the schematic (sectional view) of coupled cavities structure, which is composed of a bus waveguide coupled to multiple resonators. The indirect couplings between resonators are not discussed here. In order to control and tune Fano resonance spectra in coupled cavities system, the coupled cavities are creatively treated as a composite cavity, as shown in Fig. 1(b). An analytical theory based on the CMT[17, 21] is proposed to explore the underlying physics of spectral responses. Then, the characteristic equations for the evolutions of cavity modes can be expressed as follows

$$\frac{\partial}{\partial t}|a\rangle = -j\Omega|a\rangle - \Gamma_i|a\rangle - \Gamma_e|a\rangle + S_{+in}|K\rangle + S_{-in}|K\rangle - M|a\rangle, \tag{1}$$

$$S_{+out} = S_{+in} - \langle K|a\rangle, \tag{2}$$

$$S_{-out} = S_{-in} - \langle K|a\rangle. \tag{3}$$

$S_{\pm in}$ and $S_{\pm out}$ stand for the amplitudes of incoming and outgoing waves in bus waveguide. $|a\rangle$ and $|K\rangle$ represent field amplitude of resonant mode and coupling coefficient between resonator and bus waveguide, respectively $\langle K|$ is dependent on $|K\rangle$. They can be written as

$$|a\rangle = \begin{pmatrix} a_1 \\ a_2 \\ \vdots \\ a_N \end{pmatrix}, \quad |K\rangle = \begin{pmatrix} k_1 \\ k_2 \\ \vdots \\ k_N \end{pmatrix}, \quad \langle K| = (k_1^* \ k_2^* \ \cdots \ k_N^*),$$

where a_N denotes amplitude of the N-th mode with resonance frequency ω_N, and k_N stands for the coupling between waveguide and cavity.

In Eq. (1), Ω, Γ_i, Γ_e, and M matrixes, respectively, denote resonance frequencies, intrinsic loss rate, external loss rate of cavity, and coupling coefficients between resonant modes. They are given as

$$\Omega = \begin{bmatrix} \omega_{11} & \omega_{12} & \cdots & \omega_{1N} \\ \omega_{21} & \omega_{22} & \cdots & \omega_{2N} \\ \vdots & \vdots & \ddots & \vdots \\ \omega_{N1} & \omega_{N2} & \cdots & \omega_{NN} \end{bmatrix}, \quad \Gamma_i = \begin{bmatrix} \gamma_{i11} & \gamma_{i12} & \cdots & \gamma_{i1N} \\ \gamma_{i21} & \gamma_{i21} & \cdots & \gamma_{i2N} \\ \vdots & \vdots & \ddots & \vdots \\ \gamma_{iN1} & \gamma_{iN2} & \cdots & \gamma_{iNN} \end{bmatrix},$$

$$\Gamma_e = \begin{bmatrix} \gamma_{e11} & \gamma_{e12} & \cdots & \gamma_{e1N} \\ \gamma_{e21} & \gamma_{e22} & \cdots & \gamma_{e2N} \\ \vdots & \vdots & \ddots & \vdots \\ \gamma_{eN1} & \gamma_{eN2} & \cdots & \gamma_{eNN} \end{bmatrix}, \quad M = \begin{bmatrix} \mu_{11} & \mu_{12} & \cdots & \mu_{1N} \\ \mu_{21} & \mu_{22} & \cdots & \mu_{2N} \\ \vdots & \vdots & \ddots & \vdots \\ \mu_{N1} & \mu_{N2} & \cdots & \mu_{NN} \end{bmatrix}.$$

In Ω, Γ_i, Γ_e, and M matrixes, if $p \neq q$, $\omega_{pq} = 0$, $\gamma_{ipq} = 0$, $\gamma_{epq} = 0$, and $\mu_{pq} = \omega_{qq}/(2Q_{pq})$; if $p = q$, $\omega_{pq} = \omega_p$, $\gamma_{ipq} = \omega_{pq}/(2Q_{ip})$, $\gamma_{epq} = \omega_{pq}/(2Q_{ep})$, and $\mu_{pq} = 0$. Q_{ip}, Q_{ep}, and Q_{pq} are cavity quality factors related to intrinsic loss, waveguide coupling loss, and coupling between the pth and qth modes. Using boundary conditions of $S_{-in} = 0$ and Eqs (1–3), one can get the power transmission $T_N = |S_{+out}/S_{+in}|^2$ and power reflection $R_N = |S_{-out}/S_{+in}|^2$.

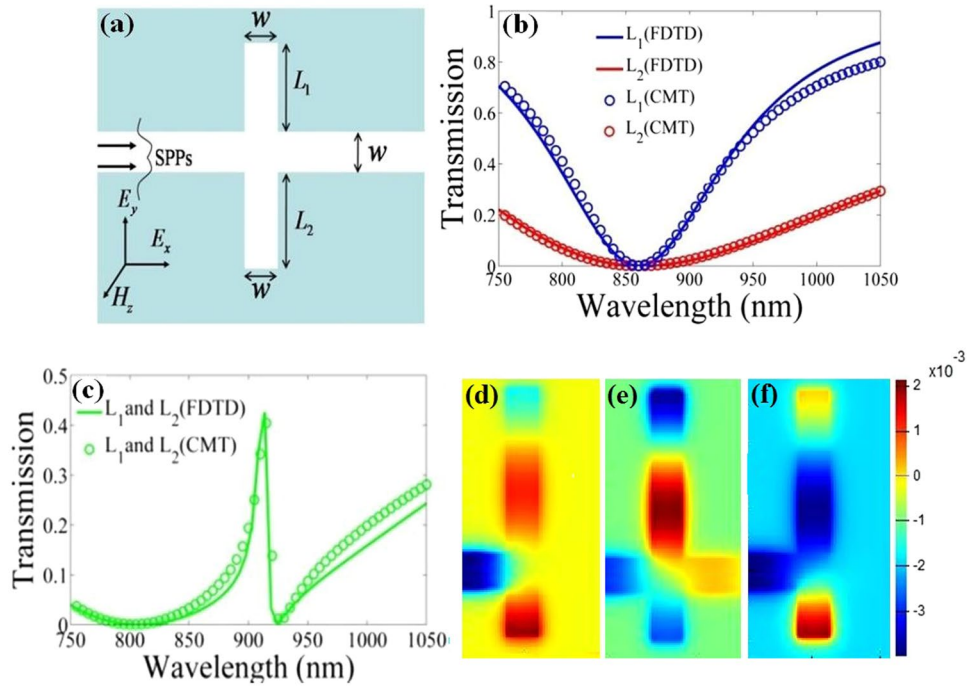When $N = 1$, the power transmission of system is written as

Figure 2. (**a**) Schematic of the plasmonic structure composed of MDM waveguide side-coupled to two stub cavities, with geometrical parameter $w = 100$ nm. (**b**) The blue line ($L_1 = 493$ nm) and red line ($L_2 = 144$ nm) correspond to transmission spectra for plasmonic resonator system with single stub. (**c**) Transmission spectra for the plasmonic stub-pair system depicted in Fig. 2(a) with $L_1 = 493$ nm and $L_2 = 144$ nm. The solid curves are simulation results and the circles are theoretical fittings. (**d**) Magnetic field distributions (H_z) at (**d**) $\lambda = 806.7$ nm, (**e**) $\lambda = 913.7$ nm, and (**f**) $\lambda = 924.4$ nm, respectively, for the plasmonic stub-pair structure.

$$T = \left| \frac{j\omega_1 - j\omega + \gamma_{i11}}{j\omega_1 - j\omega + \gamma_{i11} + \gamma_{e11}} \right|^2 . \tag{4}$$

When $N = 2$, the power transmission can be expressed as

$$T = \left| \frac{t_1 t_2 + \frac{\mu_{12}\mu_{21}}{\sigma_1\sigma_2}}{t_1 + t_2 - t_1 t_2 + \frac{\mu_{12}\mu_{21}}{\sigma_1\sigma_2} - \frac{j\mu_{12}k_1 k_2}{\sigma_1\sigma_2} - \frac{j\mu_{21}k_1 k_2}{\sigma_1\sigma_2}} \right|^2 , \tag{5}$$

where $\sigma_1 = (j\omega - j\omega_1 - \gamma_{i11} - \gamma_{e11})$, $\sigma_2 = (j\omega - j\omega_2 - \gamma_{i22} - \gamma_{e22})$, $t_1 = 1 + \gamma_{e11}/\sigma_1$, $t_2 = 1 + \gamma_{e22}/\sigma_2$.

Plasmonic stub-pair structure

To verify our theoretical model, the plasmonic stub-pair structure depicted in Fig. 2(a) is taken as an example, which consists of MDM bus waveguide side-coupled to a pair of stub resonators with the width of bus waveguide (w), length (L_1 and L_2) and width (w) of the stub resonators. The insulator and metal in the structure are, respectively, air and silver. The permittivity of silver, $\varepsilon(\omega) = 1 - \omega_p^2/(\omega^2 + i\omega\gamma_p)$, is characterized by the Drude model, with $\omega_p = 1.38 \times 10^{16}$ rad/s and $\gamma_p = 2.73 \times 10^{13}$ rad/s[34]. The perfect matched layer (PML) boundary conditions are applied to the FDTD simulations, and the spatial steps are set as 5 nm × 5 nm. With incident light polarized parallel to the stubs, surface plasmon mode can be excited and confined in waveguide. In this paper, the widths of bus waveguide and stub cavities are all equal to 100 nm, and transmittance are numerically calculated by the FDTD method.

Figure 2(b) illustrates Lorentzian-like transmission spectra for plasmonic resonator system with single stub. The blue line and red line correspond to $L_1 = 493$ nm and $L_2 = 144$ nm, respectively. For these two cases, the resonant wavelengths in Fig. 2(b) are both $\lambda = 860.2$ nm, and the full width at half maximum (FWHM) of transmission spectra are 155.2 nm and 476.3 nm, respectively. It is well known that the interference between narrowband resonant mode (for the case of single stub system with $L_1 = 493$ nm) and broadband resonant mode (for the case of single stub system with $L_2 = 144$ nm) gives rise to Fano resonance[1, 19, 29, 35]. Using the coupled-cavity structure in Fig. 2(a) with $L_1 = 493$ nm and $L_2 = 144$ nm, we obtain a sharp asymmetric Fano line shape in transmission spectra, as shown in Fig. 2(c). The transmittances for transmission dips at $\lambda = 806.7$ nm and $\lambda = 924.4$ nm are 0.00001858 and 0.00263, respectively. In Fig. 2(b) and (c), we present the comparison between the analytical and simulated transmission spectra. For analytical transmission spectra, $\omega_1 = 2.19 \times 10^{15}$ rad/s, $\omega_2 = 2.19 \times 10^{15}$ rad/s,

$Q_{i1} = 200$, $Q_{i2} = 200$, $Q_{e1} = 10$, $Q_{e2} = 3$, $Q_{12} = 10$. Obviously, the analytical results are in good agreement with the FDTD simulations, which indicates the validity of the theoretical model. Consequently, the theoretical analyses set up a platform to understand the Fano-resonance spectra in coupled cavities system, and may guide design with tunable optical responses.

To better understand the formation mechanisms of Fano line shape, Fig. 2(d–f) show the field distributions (H_z) of SPPs at different wavelengths ($\lambda = 806.7$ nm, $\lambda = 913.7$ nm, and $\lambda = 924.4$ nm) in Fig. 2(c). The field distribution in Fig. 2(e) shows that the input light at Fano resonance peak can pass through the waveguide, which arises from the destructive interference between narrowband and broadband resonant modes[1, 19, 20, 35]. Interestingly, Fig. 2(d) and (f) illustrate that the stub-pair can be taken as a composite cavity, in which the resonance modes correspond to transmission dips. Relative to bus waveguide, the mode in phase shown in Fig. 2(d) enhances the coupling between bus waveguide and composite cavity, which corresponds to broadband resonant mode and plays the role of bright mode (quasi-continuum energy state) in conventional Fano system[19]. In Fig. 2(f), the mode out of phase reduces the coupling between bus waveguide and composite cavity, which corresponds to narrowband resonant mode and plays the role of dark mode (quasi-discrete energy state). In other words, the Fano resonance line shape in the plasmonic stub-pair system can also be attributed to the interference between composite cavity modes through the MDM bus waveguide[20, 25, 29, 33].

Sensing performance based on Fano resonance

It has been proposed that the asymmetric response line shape with sharp slope in Fano resonance may find applications in label-free, ultra-sensitive, microcavity-based biosensors[21, 36]. The Fano resonance will shift to short-wavelength or long-wavelength direction when the nearby or surrounding medium changes. Here, the resonant wavelength in stub is determined by[37]

$$\lambda \approx 4n_{eff}L/(2m + 1), \tag{6}$$

where n_{eff}, L, and m ($m = 0, 1, 2, \ldots$) are, respectively, the real part of effective refractive index for SPPs[23, 26], length, and the order of resonance mode in stub resonator. The resonant wavelength is proportional to n_{eff} and L.

Then, we get

$$\frac{d\lambda}{dn_{eff}} = 4L/(2m + 1). \tag{7}$$

For a given detection wavelength, to the refractive index (n) of surrounding medium, the derivation of transmission efficiency T can be written as

$$\frac{dT}{dn} = \frac{dT}{d\lambda}\frac{d\lambda}{dn_{eff}}\frac{dn_{eff}}{dn} \propto \frac{dT}{d\lambda}. \tag{8}$$

The detection sensitivity of the plasmonic system can be defined as $|dT/dn|$. Based on Eqs (7) and (8), for simplicity, the detection sensitivity can also be expressed as[27]

$$S \equiv \left|\frac{dT}{d\lambda}\right|. \tag{9}$$

According to Eq. (9), we illustrate the sensitivity factor S (the slope of transmission spectra versus detection wavelength) as a function of detection wavelength for different plasmonic resonator system in Fig. 3(a–c). Combining Figs 2(b,c) and 3(a–c), we can conclude that the detection sensitivity S provides us a way to exhibit spectral asymmetry and investigate the sensitivity of sensor[38, 39]. For the single stub case with $L_1 = 493$ nm, the detection sensitivity in Fig. 3(a) approaches 9.256×10^6 m^{-1}, while the detection sensitivity in Fig. 3(b) reaches 3.742×10^6 m^{-1} for single stub case with $L_2 = 144$ nm, which indicates that the length of stub resonator offers an efficient way to tune the sensitivity. In Fig. 3(c), for the plasmonic stub-pair system with $L_1 = 493$ nm and $L_2 = 144$ nm, the detection sensitivity approaches 6.541×10^7 m^{-1}. That is to say, the transmission efficiency will deviate by 0.3271 even when the detection wavelength changes by less than 5 nm. Compared with the single stub in Fig. 3(a) and (b), the stub-pair apparently brings an order of magnitude enhancement in sensitivity.

Figure 4(a) shows the transmission spectra versus refractive index of surrounding medium, in which the Fano resonance shifts towards long-wavelength direction with the increase of refractive index, whereas the intensities of Fano resonance peak and resonance dip keep constant. To better characterize the performance of sensing system, the figure of merit (FOM) is one of the key parameters, which can be expressed as FOM $= [T(n + \Delta n) - T(n)]/[T(n)\Delta n] = \Delta T/(T\Delta n)$ at fixed wavelength[40–42]. ΔT denotes the transmission intensity variation, and Δn stands for the change of surrounding refractive index. $T(n + \Delta n)$ and $T(n)$ are transmission rate in nanoplasmonic structure. As refractive index increases from 1.00 to 1.01, in Fig. 4(b), we plot the FOM for plasmonic stub-pair system and two corresponding single stub structures. For the single stub case with $L_1 = 493$ nm ($L_2 = 144$ nm), the maximum FOM is about 4871 (1289); for the stub-pair system, the left and right maximum FOMs (labeled as P_1 and P_2, respectively) approach 4218 and 9673, respectively. The results indicate that coupled-cavity offers a method to improve the FOM for refractive index sensing.
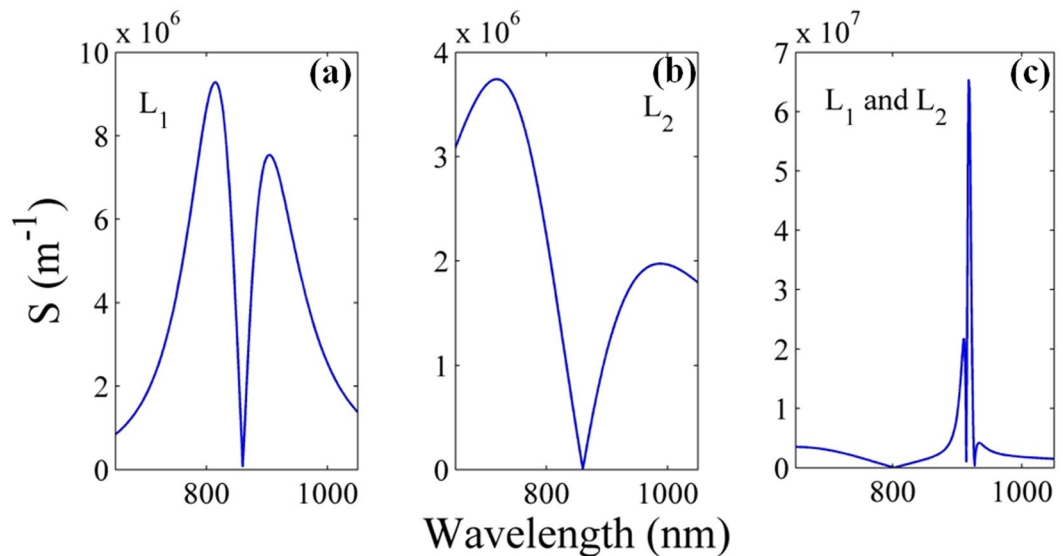
Figure 3. Sensitivity S as a function of detection wavelength for three resonator systems: (**a**) single stub L_1, (**b**) single stub L_2, (**c**) stub-pair L_1 and L_2. The system parameters are fixed as $w = 100$ nm, $L_1 = 493$ nm and $L_2 = 144$ nm.
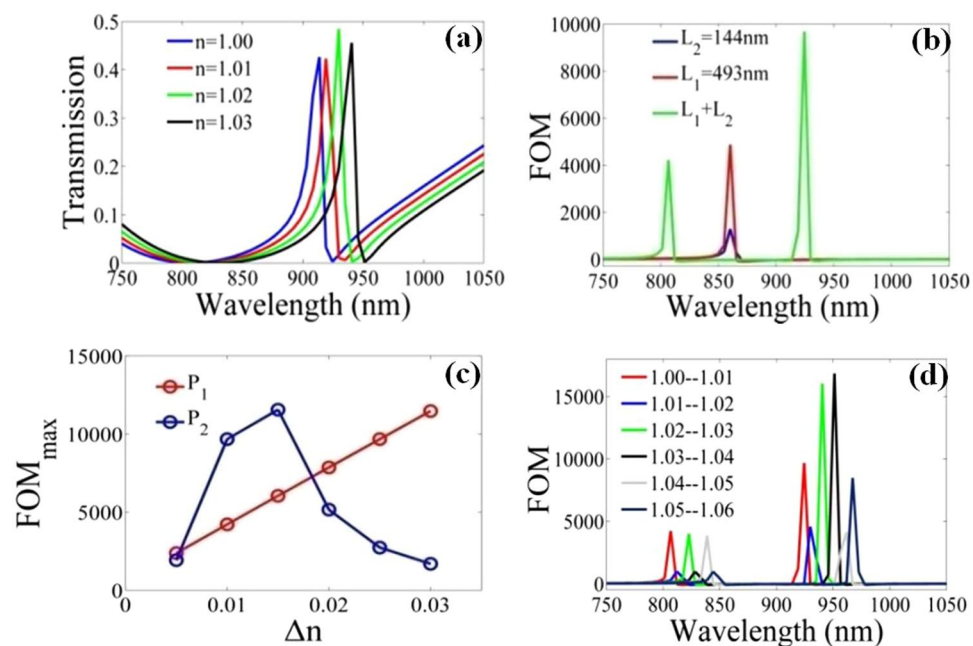

Figure 4. (**a**) Transmission spectra as a function of refractive index of surrounding medium for plasmonic stub-pair structure plotted in Fig. 2(a). (**b**) The curves of FOM for plasmonic stub-pair system (green line) and two corresponding single stub structures (blue line and red line). For the stub-pair structure, (**c**) the maximum of FOM with the change of refractive index Δn, and (**d**) the FOM curves for different ranges of refractive index. The geometrical parameters are fixed as $w = 100$ nm, $L_1 = 493$ nm and $L_2 = 144$ nm.

In order to investigate the FOM more thoroughly, for the stub-pair structure, Fig. 4(c) shows the maximum of FOM (FOM$_{max}$) versus refractive index n. According to the definition of FOM, as refractive index n increases from 1.00 to 1.03 with a step of 0.005, $T(n)$ corresponds to $T(1.00)$, and $T(n + \Delta n)$ corresponds to $T(1.005)$, $T(1.01)$, $T(1.015)$, $T(1.02)$, $T(1.025)$ and $T(1.03)$, respectively. As shown in Fig. 4(c), when refractive index n increases from 1.00 to 1.03, P_1 increases linearly, but P_2 increases first and then decreases, which means that FOM$_{max}$ is dependent on the increment of refractive index Δn. In Fig. 4(d), we present the FOM for different ranges of surrounding refractive index, such as 1.01–1.02, 1.02–1.03, 1.03–1.04, 1.04–1.05, and 1.05–1.06. In this case, the change of refractive index Δn equals 0.01, and $T(n + \Delta n)$ corresponds to $T(1.01)$, $T(1.02)$, $T(1.03)$, $T(1.04)$, $T(1.05)$ and $T(1.06)$, respectively. It can be obtained that the maximum of P_1 increases and decreases
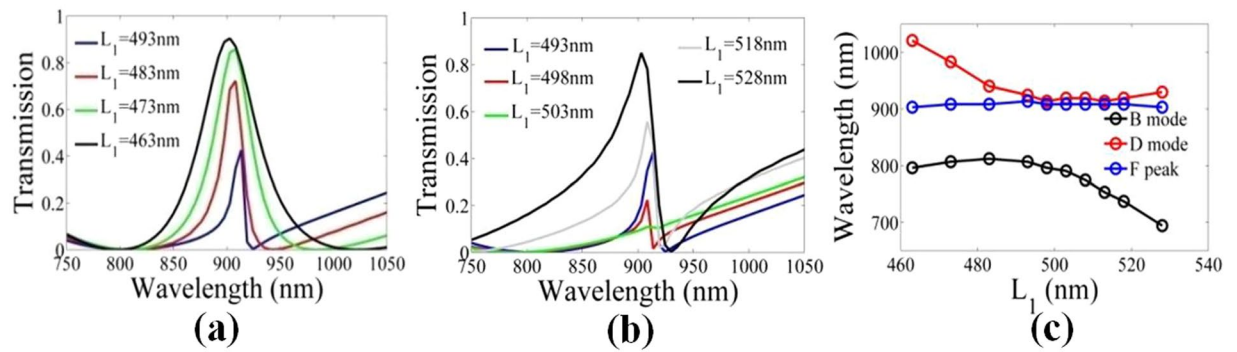
Figure 5. Transmission spectra (**a**) and (**b**) for plasmonic structure in Fig. 2(a) as a function of L_1. (**c**) Wavelengths of bright mode (B mode, black line), dark mode (D mode, red line), and Fano peak (F peak, blue line). The other structure parameters are fixed as $w = 100$ nm, $L_1 + L_2 = 637$ nm.

alternately, while P_2 approaches 1.6×10^4 in the ranges of 1.02–1.03 and 1.03–1.04. That is to say, the sensing performances are also related to the range of refractive index. These results may lay a basis for fundamental research of ultra-compact plasmonc sensor applications.

It is well known that spectral asymmetry plays a critical role in applications of Fano resonance. Therefore, the control of Fano line shape has been a topic of investigations. Because the Fano resonance arises from the interference between dark mode (narrowband resonant mode) and bright mode (broadband resonant mode), independent control of resonant mode is useful for precise control of Fano resoance in highly integrated optical circuits. In Fig. 5(a) and (b), we present the transmission spectra versus L_1 for the plasmonic stub-pair system. The other constructive parameters are fixed as $w = 100$ nm, $L_1 + L_2 = 637$ nm. Obviously, the asymmetry of Fano resonance line shape can be adjusted by L_1. To better investigate the evolution of spectral asymmetry versus L_1, we display the wavelengths of bright mode (black line), dark mode (red line), and Fano peak (blue line) as a function of L_1 in Fig. 5(c). As can be clearly seen, when L_1 increases from 463 nm to 528 nm, the Fano peak wavelength is nearly unchanged; when L_1 increases from 463 nm to 493 nm, the wavelength gap between bright mode (dark mode) and Fano peak is nearly constant (becomes smaller); when L_1 increases from 493 nm to 528 nm, the wavelength gap between bright mode (dark mode) and Fano peak becomes larger (is unchanged). As mentioned above, with constant sum of L_1 and L_2 in the plasmomic stub-pair structure, the wavelengths of bright mode and dark mode can be adjusted independently by L_1, which provides an additional degree of freedom to control the slope of Fano resonance spectra and, thus, indicates the tunability of detection sensitivity in the plasmonic nanostructure.

Conclusion

In summary, we have analytically and numerically investigated tunable and high-sensitivity sensing performances based on Fano resonance in plasmonic coupled cavities system. Based on the CMT, the coupled cavities can be taken as a composite cavity. Using the plasmonic stub-pair structure as an example, the analytical spectral responses are consistent with the FDTD simulations, which confirms our theoretical model, and implies that Fano resonance line shape in plasmonic stub-pair system results from the interference between composite cavity modes through MDM bus waveguide[19, 20, 33]. The detection sensitivity factor in coupled cavities approaches $6.541 \times 10^7 \, \text{m}^{-1}$, and is an order of magnitude larger than single stub case. Moreover, the effects of structure parameters and surrounding medium play important roles on sensing performances. In particular, the wavelengths of bright mode and dark mode in the plasmomic stub-pair structure can be adjusted independently, which may open up avenues for improving detection sensitivity. These results may be helpful for realizing high-sensitivity sensor in integrated optical circuits.

Methods

The relative permittivity of silver is described by the Drude model: $\varepsilon(\omega) = \varepsilon_\infty - \omega_p^2/(\omega^2 + i\omega\gamma_p)$, with the dielectric constant at infinite angular frequency $\varepsilon_\infty = 3.7$, the bulk plasma frequency $\omega_p = 1.38 \times 10^{16}$ rad/s and the electron collision frequency $\gamma_p = 2.73 \times 10^{13}$ rad/s. The spectral responses of the structure are investigated with the FDTD method using FDTD Solutions. The calculation domain is surrounded by perfectly matched layer (PML) absorbing boundary, and the simulation parameters have been given in our paper.

References

1. Miroshnichenko, E., Flach, S. & Kivshar, Y. S. Fano resonances in nanoscale structures. *Rev. Mod. Phys.* **82**, 2257–2298 (2010).
2. Luk'yanchuk, B. *et al*. The Fano resonance in plasmonic nanostructures and metamaterials. *Nat. Mater.* **9**, 707–715 (2010).
3. Verellen, N. *et al*. Fano resonances in individual coherent plasmonic nanocavities. *Nano Lett.* **9**, 1663–1667 (2009).
4. Wu, C. *et al*. Fano-resonant asymmetric metamaterials for ultrasensitive spectroscopy and identification of molecular monolayers. *Nat. Mater.* **11**, 69–75 (2012).
5. Chang, W. S. *et al*. A plasmonic Fano switch. *Nano Lett.* **12**, 4977–4982 (2012).
6. Qiu, W. T., Ndao, A., Lu, H. H., Bernal, M. P. & Baida, F. I. Guided resonances on lithium niobate for extremely small electric field detection investigated by accurate sensitivity analysis. *Opt. Express* **24**, 20196–20209 (2016).

7. Zhao, J., Zhang, C., Braun, P. V. & Giessen, H. Large-area low-cost plasmonic nanostructures in the NIR for Fano resonant sensing. *Adv. Mater.* **24**, 247–252 (2012).
8. Mukherjee, S. *et al*. Fanoshells: nanoparticles with built-in Fano resonances. *Nano Lett.* **10**, 2694–2701 (2010).
9. Hao, F., Nordlander, P., Sonnefraud, Y., Dorpe, P. V. & Maier, S. A. Tunability of subradiant dipolar and Fano-type plasmon resonances in metallic ring/disk cavities: implications for nanoscale optical sensing. *ACS Nano* **3**, 643–652 (2009).
10. Wu, S. H. *et al*. Cell viability monitoring using Fano resonance in gold nanoslit array. *Appl. Phys. Lett.* **103**, 133702 (2013).
11. Belotelov, V. I. *et al*. Enhanced magneto-optical effects in magnetoplasmonic crystals. *Nat. Nanotechnol.* **6**, 370–376 (2011).
12. Christ, A. *et al*. Controlling the Fano interference in a plasmonic lattice. *Phys. Rev. B* **76**, 201405 (2007).
13. Cai, W. S., Shin, W., Fan, S. H. & Brongersma, M. L. Elements for plasmonic nanocircuits with threedimensional slot waveguides. *Adv. Mater.* **22**, 5120–5124 (2010).
14. Neutens, P., Van Dorpe, P., De Vlaminck, I., Lagae, L. & Borghs, G. Electrical detection of confined gap plasmons in metal-insulator-metal waveguides. *Nat. Photonics* **3**, 283–286 (2009).
15. Salamin, Y. *et al*. Direct conversion of free space millimeter waves to optical domain by plasmonic modulator antenna. *Nano Lett.* **15**, 8342–8346 (2015).
16. Han, Z. H. & Bozhevolnyi, S. I. Radiation guiding with surface plasmon polaritons. *Rep. Prog. Phys.* **76**, 016402 (2013).
17. Haus, H. A. Waves and fields in optoelectronics (Prentice-Hall, New Jersey, 1984).
18. Min, C. & Veronis, G. Absorption switches in metal–dielectric–metal plasmonic waveguides. *Opt. Express* **17**, 10757–10766 (2009).
19. Li, B. B. *et al*. Experimental observation of Fano resonance in a single whispering-gallery microresonator. *Appl. Phys. Lett.* **98**, 021116 (2011).
20. Cao, G. T., Li, H. J., Zhan, S. P., He, Z. H. & Li, B. X. Plasmon-induced transparency in a single multimode stub resonator. *Opt. Express* **22**, 25215–25223 (2014).
21. Li, J. H., Yu, R., Ding, C. L. & Wu, Y. *PT*-symmetry-induced evolution of sharp asymmetric line shapes and high-sensitivity refractive index sensors in a three-cavity array. *Phys. Rev. A* **93**, 023814 (2016).
22. Huang, Y., Min, C. J. & Veronis, G. Broadband near total light absorption in non-PT-symmetric waveguide-cavity systems. *Opt. Express* **24**, 22219–22231 (2016).
23. Lu, H., Liu, X. M. & Mao, D. Plasmonic analog of electromagnetically induced transparency in multinanoresonator-coupled waveguide systems. *Phys. Rev. A* **85**, 053803 (2012).
24. Yu, Z. F., Veronis, G., Fan, S. H. & Brongersma, M. L. Gain-induced switching in metal-dielectric-metal plasmonic waveguides. *Appl. Phys. Lett.* **92**, 041117 (2008).
25. He, Z. *et al*. Theoretical analysis of ultrahigh figure of merit sensing in plasmonic waveguides with a multimode stub. *Opt. Lett.* **41**, 5206–5209 (2016).
26. Cao, G. T. *et al*. Uniform theoretical description of plasmon-induced transparency in plasmonic stub waveguide. *Opt. Lett.* **39**, 216–219 (2014).
27. Xiao, Y. F., Gaddam, V. & Yang, L. Coupled optical microcavities: an enhanced refractometric sensing configuration. *Opt. Express* **16**, 12538–12543 (2008).
28. Fan, S. H. Sharp asymmetric lineshapes in side-coupled waveguide–cavity systems. *Appl. Phys. Lett.* **80**, 908–910 (2002).
29. Xiao, Y. F. *et al*. Asymmetric Fano resonance analysis in indirectly coupled microresonators. *Phys. Rev. A* **82**, 065804 (2010).
30. Lu, H., Liu, X. M., Mao, D. & Wang, G. X. Plasmonic nanosensor based on Fano resonance in waveguide-coupled resonators. *Opt. Lett.* **37**, 3780–3782 (2012).
31. Chen, L. *et al*. Numerical analysis of a near-infrared plasmonic refractive index sensor with high figure of merit based on a fillet cavity. *Opt. Express* **24**, 9975–9983 (2016).
32. Huang, Y., Min, C. J., Dastmalchi, P. & Veronis, G. Slow-light enhanced subwavelength plasmonic waveguide refractive index sensors. *Opt Express* **23**, 14922–14936 (2015).
33. Xiao, Y. F., He, L., Zhu, J. & Yang, L. Electromagnetically induced transparency-like effect in a single polydimethylsiloxane coated silica microtoroid. *Appl. Phys. Lett.* **94**, 231115 (2009).
34. Palik, E. D. Handbook of optical constants in solids (Academic, 1982).
35. Chen, J. J. *et al*. Tuning Fano resonances with a nano-chamber of air. *Opt. Lett.* **41**, 2145–2148 (2016).
36. Wang, C. & Search, C. P. Nonlinearly enhanced refractive index sensing in coupled optical microresonators. *Opt. Lett.* **39**, 26–29 (2014).
37. Tao, J., Hu, B., He, X. Y. & Wang, Q. J. Tunable subwavelength terahertz plasmonic stub waveguide filters. *IEEE Trans. Nanotechnol.* **12**, 1191–1197 (2013).
38. He, G. Z. Coll. Math. **25**, 196–198, (2009).
39. Fichtenholz, G. M. Differential and integral calculus I (Higher Education, Beijing, 2006).
40. Bera, M. & Ray, M. Circular phase response based analysis for swapped multilayer metallo-dilelectric plasmonic structures. *Plasmonics* **9**, 237–249 (2014).
41. Ameling, R. *et al*. Cavity-enhanced localized plasmon resonance sensing. *Appl. Phys. Lett.* **97**, 253116 (2010).
42. Roh, S., Chung, T. & Lee, B. Overview of the characteristics of micro- and nano-structured surface plasmon resonance sensors. *Sensors* **11**, 1565–1588 (2011).

Acknowledgements

Author Contributions

X.C. and W.L. supervised the project, Y.D. and G.C. performed numerical simulation, analyzed the data and edited the figures. H.Y. and G.L. gave some valuable suggestions on analyzing the data. All authors participated in the discussion of the project. Y.D. and G.C. wrote the manuscript with contributions from all authors.

Additional Information

Competing Interests: The authors declare that they have no competing interests.

Publisher's note: Springer Nature remains neutral with regard to jurisdictional claims in published maps and institutional affiliations.